RSC Advances

This is an *Accepted Manuscript*, which has been through the Royal Society of Chemistry peer review process and has been accepted for publication.

Accepted Manuscripts are published online shortly after acceptance, before technical editing, formatting and proof reading. Using this free service, authors can make their results available to the community, in citable form, before we publish the edited article. This *Accepted Manuscript* will be replaced by the edited, formatted and paginated article as soon as this is available.

You can find more information about *Accepted Manuscripts* in the **Information for Authors**.

ROYAL SOCIETY OF CHEMISTRY

www.rsc.org/advances

Young's modulus and Poisson's ratio for TiO$_2$-based Nanotubes and Nanowires: Modelling of Temperature dependence.

Sergey I. Lukyanov[*], Andrei V. Bandura, Robert A. Evarestov

St. Petersburg State University, 7/9 Universitetskaya nab., St. Petersburg, 199034, Russia.

In this work the molecular mechanics simulations with the help of interatomic potentials were employed to predict temperature dependence of the Young's modulus and Poisson's ratio of a number of TiO$_2$ –based four facetted nanotubes and nanowires. The temperature dependence of the Young's modulus was obtained through the calculation of the Helmholtz free energy of the system under the isothermal thermodynamic conditions. The Helmholtz free energy simulations were performed in the framework of quasi-harmonic approximation as a result of calculations of the potential energy and the harmonic phonon frequencies of the system under consideration. The Helmholtz free energy calculated for the set of fixed values of the nanoobject translational period allows obtaining the minimal Helmholtz free energy at specified temperatures in the range 0-1000 K. The present simulations demonstrate that the Young's modulus for the TiO$_2$ –based nanowires decrease with the increase of the nanowire diameters and approaches to the modulus for the rutile bulk crystal from above. Also, the temperature behavior of the Young's modulus, Poisson's ratio and period for the nanotubes and nanowires are considered. This study reveals that the Poisson's ratios of the nanotubes and nanowires depend on the surface atoms chosen to measure the transverse dimensions of the nanostructures.

Introduction

Mechanical properties of TiO$_2$-based nanostructures (nanotubes – NTs and nanowires - NWs) are important due to their practical applications. In particular, the strengthening of polystyrene films with small amounts of the TiO$_2$-based nanotubes enables the increase of the Young's modulus of the nanohybrid films by 18% and the tensile strength by 30%.[1] In medicine, the treatment of the surface of metallic titanium implant by TiO$_2$ nanotubes improves osteointegration of the implant and prevents dislocation and premature loosening. The stability of the implant surface is determined by the elastic modulus of TiO$_2$ nanotubes and nanowires.[2-4]

Titania nanowires have exceptional photocatalytic and photovoltaic activity, outstanding optical properties.[5] Mechanical characteristics of NWs is very important to understand the possibility of developing the reliable photovoltaic and photocalytic cells, optical and electrical devices based on titania nanowires.[6]

Experimental measurements of the elastic properties of the nanostructures based on ZnO, TiO$_2$ and other inorganic compounds give strongly different results.[6-11] Additional information on the behavior of TiO$_2$ nanostructures under mechanical loads at different temperatures can be obtained by theoretical modeling of the temperature dependence of the Young's modulus.

---

[*] *e-mail: s.lukyanov@spbu.ru*

A number of computer-aided studies has been performed to investigate the temperature dependence of the mechanical properties of the single-walled, double-walled carbon nanotubes[12-16] and carbon-based nanomaterials such as the fullerene and nanotube derivatives.[17] The main approaches used in these works are the classical molecular dynamics with empirical potentials and density-functional-based tight binding (DFTB) molecular dynamics.[12,13,16] The temperature dependence of the Young's modulus, Y, for the nanotubes has been simulated using the determination of strain for a fixed stress[16,17] and the determination of stress for a fixed strain techniques.[17-19] Also, the temperature dependence of the stiffness of single-walled carbon nanotubes has been estimated by the molecular dynamics simulations of the intrinsic thermal vibrations of a single-walled carbon nanotube modelled as a clamped cantilever.[12] The Young's modulus values were calculated from the equation relating the modulus and standard deviation of the vibrational amplitude of the tube's free tip displacement.

The results of Dereli and Süngü[14] indicate that the Young's modulus of (10, 10) nanotube decreases in the interval 0 K$<T<$1000 K but increases at temperature higher than 1000 K. The (10, 10) nanotube also has been studied by Zhang and Shen.[13] The authors of mentioned papers employed different values of the nanotube's wall thickness δ. For comparing the results one can use an area-based Young's modulus $Y_S=Y\delta$.[20] Our comparison of these studies' results reveals that the Y_S values may differ by as much as 2.8 times.

Jin-Yuan Hsieh et al[12] investigated the carbon zig-zag nanotubes (n, 0) with n=7, 9, 12 and higher and a (5, 5) armchair nanotube. As follows from Figure 3 of this paper,[12] the Young's modulus of almost all considered nanotubes are invariable or demonstrate small growth in temperature interval from 100 K to 1000 K.

In the work of H. Jiang et al[21] a finite-temperature constitutive model not involving molecular dynamics simulation was established. The model using harmonic vibrational frequency and quasi-harmonic approximation[22] allows one to simulate the Helmholtz free energy and to compute the temperature dependence of the mechanical properties for the nanosystem. This model has been applied to the investigation of the Young's modulus and Poisson ratio of graphene.

In recent years the investigations of the mechanical properties of the inorganic nanotubes[23-27] and nanowires[11,28-32] have been carried out. However, to the best of our knowledge, the only study on the temperature dependence of the mechanical properties of the inorganic nanoobjects is published in our recent article.[33]

2

Our previous paper[33] presents the results of the study of the Young's modulus temperature dependence of the TiO_2-based cylindrical single-walled nanotubes with zig-zag and armchair chiralities and nanotubes with consolidated single wall (CSW NT). The latter are obtained from the cylindrical coaxial double-walled NTs by merging the single-walled constituents. The cylindrical single-walled constituents of the NTs were rolled up from the (111) 3-plane slab cut from a fluorite phase TiO_2 crystal, space group $Fm\bar{3}m$.

The used[33] quasi-harmonic approximation and Helmholtz free energy simulation based on harmonic vibrational frequency is more simple method than the molecular dynamics modelling and it can produce the consistent results.

The present paper has five parts. In the section "Method" the theoretical background of the elastic moduli calculations and relevant formulae are described. The section "Nanostructure models and Computational Details" presents the nanoobject models used and describes the applied atom-atom force field and specific characteristics of the computational procedure. The analysis of the obtained data and the discussion of the results are arranged in the section "Results and Discussion". The summary of the present study conclusions is given in the last section "Conclusions".

Method

One of the main mechanical characteristics of a nanotube is the Young's modulus:

$$Y = \frac{\sigma}{\varepsilon_\parallel} = \frac{\sigma}{(\Delta L/L_0)}, \tag{1}$$

where $\sigma = F/S$ is the stress or uniaxial pressure due to the force F applied along the nanotube axis and S is the cross-sectional area. The strain along the nanotube axis $\varepsilon_\parallel$ is defined as follows:

$$\varepsilon_\parallel = (L - L_0)/L_0 \tag{2}$$

where L_0 is the initial length of the unit cell or period of the unstrained monoperiodic nanotube; L is the period of the nanotube under strain. The Eq. (1) is following from the consideration of the thermodynamics of the distortion of a solid. Also, as one of the results, this consideration leads to the important thermodynamics relation:

$$\sigma = \left(\frac{\partial E}{\partial \varepsilon_\parallel}\right)_S = \left(\frac{\partial F}{\partial \varepsilon_\parallel}\right)_T, \tag{3}$$

where T is a temperature, E is the total internal energy of the nanosystem, S is the entropy, F Helmholtz free energy.[34]

Combining Eq. (1) and (2) one can get

$$Y(T) = \frac{1}{V_0(T)} \left(\frac{\partial^2 E(T)}{\partial \varepsilon_\parallel^2(T)} \right)_{S, \varepsilon_\parallel = 0} \tag{4a}$$

$$Y(T) = \frac{1}{V_0(T)} \left(\frac{\partial^2 F(T)}{\partial \varepsilon_\parallel^2(T)} \right)_{T, \varepsilon_\parallel = 0}, \tag{4b}$$

where $V_0(T)$ is the volume of the unstrained nanosystem since the energies E and F must be related to the unit volume.

To obtain the Young's modulus from the results of computer simulation the change in the total internal energy of the nanosystem during an isothermal process is frequently applied as follows.[25,27]

$$Y(T) = \frac{1}{V_0(T)} \left(\frac{\partial^2 E(T)}{\partial \varepsilon_\parallel^2(T)} \right)_{T, \varepsilon_\parallel = 0} \tag{4c}$$

However the more correct way to compute the Young's modulus $Y(T)$ considering an isothermal process is to use the Eq. (4b).

The second quantity describing the mechanical properties of the nanostructures is the Poisson's ratio:

$$\nu = -\frac{\varepsilon_\perp}{\varepsilon_\parallel}. \tag{5}$$

The transverse strain $\varepsilon_\perp$ appears as a respond to exerting the longitudinal stress or uniaxial pressure σ on the nanostructure. The strain $\varepsilon_\perp$ is defined as follows:

$$\varepsilon_\perp = (D - D_0)/D_0, \tag{6}$$

where D_0 is the initial size of the nanostructure in the direction perpendicular to the nanotube or nanowire axis; D is this transvers size due to the longitudinal stress σ. Using Eqs. (2), (5), (6) and taking into account $\Delta L = (L - L_0)$ and $\Delta D = (D - D_0)$ as infinitesimal quantities the Poisson's ratio can be written in a differential form as (also see the Eq. (4)[26])

$$\nu(T) = -\frac{L_0(T)}{D_0(T)} \left(\frac{\partial D}{\partial L} \right)_{L_0(T)}. \tag{7}$$

The Young's modulus and the Poisson's ratio are independent elastic properties.[35]

The molecular mechanics (MM) modelling of the structural and mechanical properties of the nanosystems has been carried out by us with the help of GULP program package.[36] Using an empirical force field the potential energy and the phonon harmonic frequencies of the considered nanotubes and nanowires were calculated. The calculated in harmonic

4

approximation vibrational frequencies of the considered nanotubes or nanowires have been computed to obtain the temperature-dependent Helmholtz free energy. The temperature-dependent Helmholtz free energy is the sum of zero point vibrational energy E_0 and the contribution of the temperature-dependent free harmonic phonon energy $F(T)$. The zero point energy and the Helmholtz free energy are given by the well-known equation:

$$E_0 = \frac{1}{N_{\mathbf{k}}} \sum_{\mathbf{k}}^{N_{\mathbf{k}}} \sum_{i=1}^{N_v} n_i \frac{h v_i(\mathbf{k})}{2}, \tag{8a}$$

$$F = U + E_0 + F(T) = U + \frac{1}{N_{\mathbf{k}}} \sum_{\mathbf{k}}^{N_{\mathbf{k}}} \sum_{i=1}^{N_v} n_i \left[\frac{h v_i(\mathbf{k})}{2} + k_{\mathrm{B}} T \ln\{1 - \exp[-(h/k_{\mathrm{B}}) v_i(\mathbf{k})/T]\} \right], \tag{8b}$$

where k_{B} is the Boltzmann constant, h is the Plank constant, $v_i(\mathbf{k})$ is ith mode frequency, cm^{-1}, n_i is ith mode degeneracy, $N_{\mathbf{k}}$ is the number of $\mathbf{k}$-points in Brillouin Zone (BZ), N_v is the number of vibrational modes, E_0 is the zero point energy, U is the potential energy. In our calculations, the summation in Eq. (8) is made over 16 points uniformly distributed over the monoperiodic BZ of the nanotube.

The optimization of the atomic structure of the nanowire or nanotube is the first step of the elastic moduli simulation using quasi-harmonic approximation.[22] Thus, the period of the optimized structure L^* corresponds to the minimal potential energy of the system: the term U in Eq. 8. To obtain the dependence of the energy and transvers strain $\varepsilon_\perp$ on the axial strain $\varepsilon_\parallel$ seven contracted and nine elongated samples have been considered: $L_i = L^*(1 + i\Delta\varepsilon_\parallel)$; i = -7, …, 0, 1, …, 9. The strain step $\Delta\varepsilon_\parallel = 0.003$ was taken the same as in molecular dynamics simulations of the Young's modulus for the carbon nanotubes.[19]

For each sample the period L_i was fixed and potential energy minimization procedure executed to get the optimized atomic structure in local minimum of the potential energy $U(\varepsilon_{\parallel,i}^*)$. The Helmholtz free energy was calculated according to Eq. 8a for every optimized structure of the initial, contracted and elongated samples. The calculations were done at temperatures T_j in the temperature interval from 0 K to 200 K with the step $\Delta T = 25$ K and in the interval from 200 K to 1000 K with the step $\Delta T = 50$ K. A number of data sets $F(\varepsilon_{\parallel,i}^*, T_j)$ with $\varepsilon_{\parallel,i}^* = (L_i - L^*)/L^*$ and T_j from the abovementioned temperature interval have been obtained. A five-degree polynomial was fitted to every Helmholtz free energy data set $F(\varepsilon_{\parallel,i}^*, T_j)$ at fixed temperature T_j. These polynomials allow one to calculate the second derivative of $F(\varepsilon_\parallel^*, T_j)$ in respect to tensile uniaxial strain $\varepsilon_\parallel^*$.

The minimum of $U(\varepsilon_{\parallel}^{*})$ is located at $\varepsilon_{\parallel}^{*}=0$ and independent of T, whereas a position of the $F(\varepsilon_{\parallel}^{*}, T_{j})$ minimum does not coincide with that of $U(\varepsilon_{\parallel}^{*})$ $\varepsilon_{\parallel}^{*}=0$ and changes with T increase. As discussed above, the Young's modulus can be obtained using Eq. 4b, where the Helmholtz energy is a function of strain $\varepsilon_{\parallel}^{0,T}=(L-L_{0,T})/L_{0,T}$ and $L_{0,T}$ is the period of the unstrained nanostructure with a the minimal Helmholtz free energy at temperature T. The relationship between the periods L^{*} and $L_{0,T}$ can easily be obtained: $L_{0,T}=L^{*}(\varepsilon_{\parallel}^{0,T}+1)$. The relation between the second derivatives of F in respect to $\varepsilon_{\parallel}^{*}$ and in respect to $\varepsilon_{\parallel}^{0,T}$ is as follows:

$$\left(\frac{\partial^2 F}{\partial \varepsilon_{\parallel}^{0,T\,2}}\right)_{T,\varepsilon=0} = \left(\frac{L_{0,T}}{L^{*}}\right)^2 \left(\frac{\partial^2 F}{\partial \varepsilon_{\parallel}^{*\,2}}\right)_{T,\varepsilon=0}. \tag{9}$$

The usage of the unit cell parameters corresponding to the Helmholtz free energy minimum at fixed temperature determines the quasi-harmonic approximation. To find Helmholtz free energy minimum the vibrational frequencies are calculated for the certain range of the unit cell parameters. At the same time, the vibrational frequencies is obtained assuming that the atomic vibrations are harmonic.

Also, for each sample the transvers size of the sample D_i and, consequently, the data set $D_i(L_i)$ was obtained. A quadratic polynomial was fitted to the $D_i(L_i)$ data set, that allows one to calculate the transvers size $D^{0,T}$ and the derivative $\left(\partial D/\partial L\right)_{L_{0,T}}$ corresponding to $L_{0,T}$. The Poisson's ratio at temperature T was calculated according to the equation

$$\nu(T) = -\frac{L_{0,T}}{D^{0,T}}\left(\frac{\partial D}{\partial L}\right)_{L_{0,T}}. \tag{10}$$

Nanostructure models and Computational Details

As it was shown in our earlier study[37] the double- and triple-walled cylindrical coaxial TiO$_2$-based NTs merge producing NTs with consolidated single wall. Depending on the NTs chirality and an interwall distance, the resulting consolidated single wall consists of planar and/or curved sections of the slab together with some elements of the rutile structure as in Figure 1a. However it appears that modelling of the NTs elongation and compression allows us to perform a more detailed study of the NT potential energy surface and, in some cases, to find an optimized structure with lower potential energy. In that way in our present work a more stable optimized structure of the (8, 8)@(12, 12)@(16, 16) CSW NT with 72 TiO$_2$ formula units (FU) per NT unit cell (UC) was been obtained, see Figure 1b. One can see from Figure 1b that this more stable structure is very close to the one of the rutile-based four

facetted nanotubes (FNT) shown in Figure 2a and contains 72 FU per UC. In one's turn this four facetted nanotube is obtained through cutting a smallest (9 TiO_2 FU per UC) four facetted Ti atom centered nanowire from a largest (81 FU per UC) four facetted nanowire (FNW), see Figures. 3a and 2b, respectively. Both nanowires under consideration, largest and smallest ones, are cut from rutile titania bulk along the [001] direction passing through Ti atoms.[5]
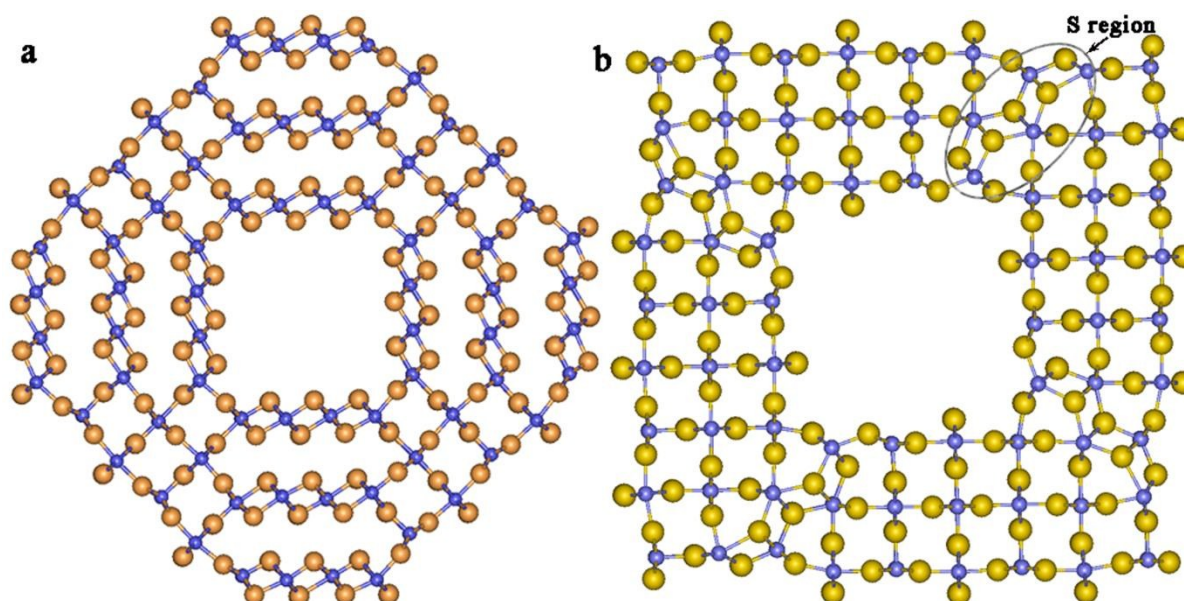

Figure 1. Cross-section images of the (8, 8)@(12, 12)@(16, 16) CSW NT with 72 FU per UC: a) an intermediate structure; b) the distorted FNT structure with minimum potential energy. Larger light spheres are oxygen ions, smaller dark spheres are titanium ions.

The largest part of the wall of CSW NT consists of the rutile-like elements. The small number of the fluorite-like elements (see region S in Figure 1b) is included in the nanotube's wall and distorts the structure which is basically similar to the structure of the four-facetted NT, Figure 2a. In that way the (8, 8)@(12, 12)@(16, 16) CSW NT can be defined as a distorted four facetted NT. The morphology[38] and electronic properties[39] of anatase-based facetted NTs and rutile-based facetted NWs have been considered. The structural and electronics properties of [001]-oriented Ti atom-centered and hollow site-centered NWs have been investigated by large-scale ab initio Density Functional Theory (DFT) and hybrid DFT–Hartree Fock (DFT–HF) calculations.[40]

In that way, the subject of the present study is the calculation of the elastic properties temperature dependence of the seven objects: two nanotubes (distorted four facetted NT with 72 formula units per UC, (Figure 1b), four facetted NT with 72 FU per UC, (Figure 2b)) and five nanowires (four facetted [001]-oriented Ti atom-centered NWs with 81, 9, 25 (middle

FNW) FU per UC, Figures 2b, 3a, 3b, and hollow site-centered NWs with 16 (small FNW), 64 (large FNW) FU per UC, (Figures 3c, 3d).
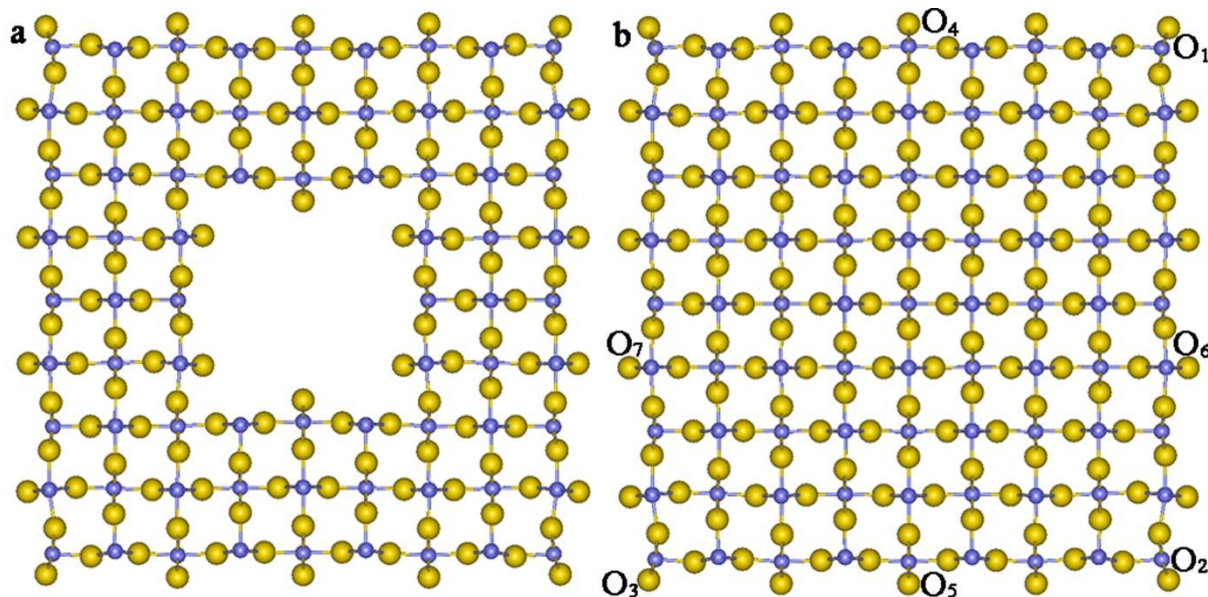

Figure 2. Cross-sectional images of the nanostructures of rutile morphology: a) FNT with 72 formula units per UC and b) FNW with 81 formula units per UC, largest. O_1, O_2, O_3 are corner oxygen atoms; O_4, O_5, O_6 and O_7 are edge oxygen atoms.

A lot of atom-atom interaction potentials have been developed for simulating a variety of structures and diverse properties of the different polymorphs of TiO_2. These force fields were employed in the Monte Carlo,[41] molecular mechanics and molecular dynamics studies[42-49] of the crystals. We have tested the ability of these different force fields to reproduce the values of the structural and mechanical parameters and phonon frequencies of four known phases of TiO_2 crystals: rutile, anatase, brookite, and columbite. In addition, we tested the ability of the force fields to reproduce the structure and phonon frequencies of the (111) 3-plane slab of a fluorite-like TiO_2 crystal and two cylindrical nanotubes (6, 6) and (12, 12) rolled up from such a slab. As far as we know, there are no the experimental data on the properties of the mentioned fluorite layer and two nanotubes. Therefore values of the structural parameters and phonon frequencies of the slab and nanotubes were obtained from our DFT calculations. The practice of employing the results of quantum chemical studies for parameterization of the force fields is widely used.[48,50,51]

Our comparison of DFT and force field calculations results shows that the lattice parameters and mechanical properties of the four mentioned polymorphs of TiO_2 are reproduced well by the force field of Kim et al[46] and, slightly worse, by the one of Matsui and Akaogi (M&A).[45] However, the phonon frequencies of these TiO_2 phases and nanotubes are reproduced more accurately by means of the M&A interaction potential. Thus, the force field

used in the present work is a set of atom-atom interaction potentials developed by Matsui and Akaogi[45] with the use of the molecular dynamics modeling.
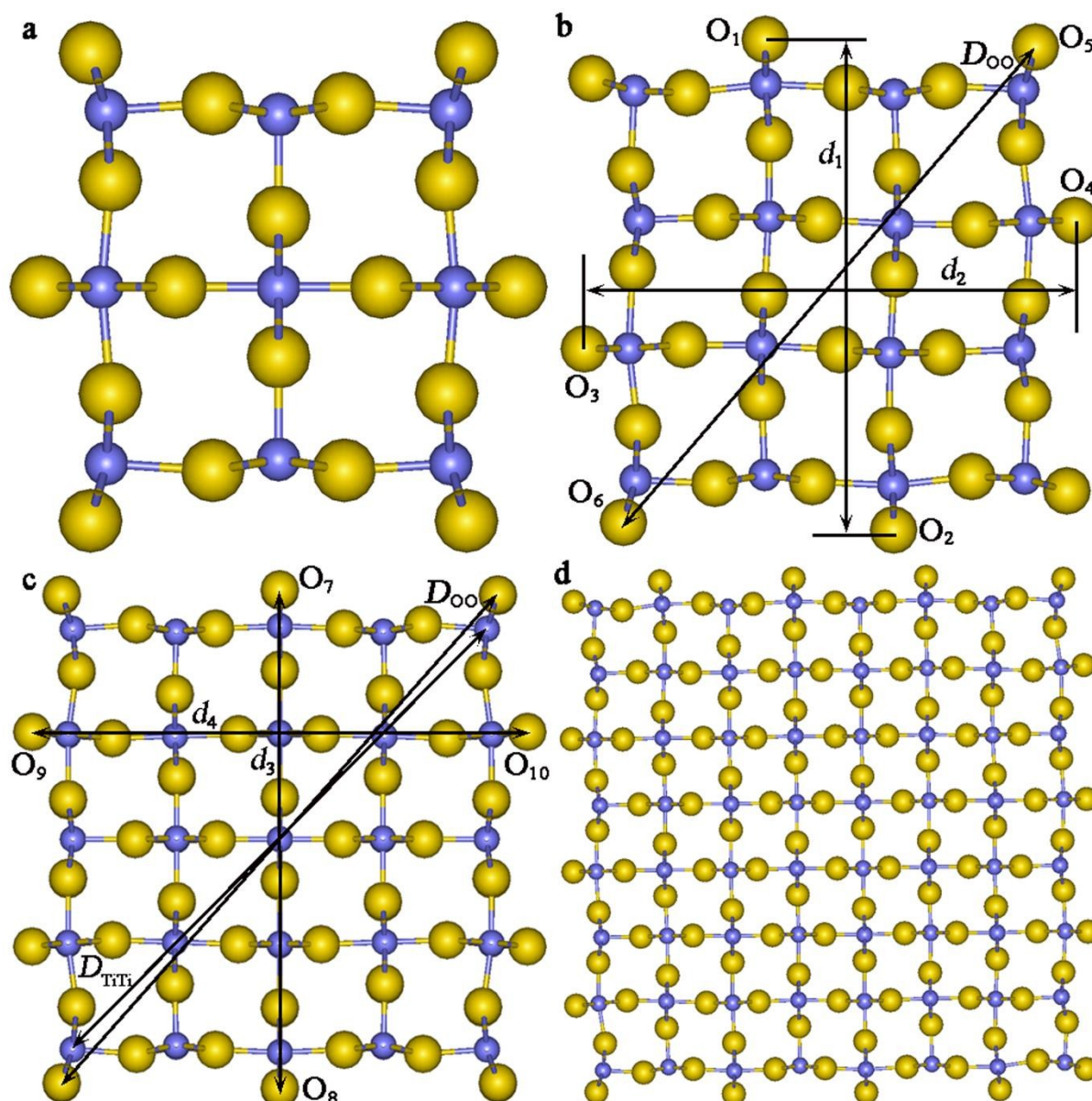

Figure 3. Cross-sectional images of the nanowires of rutile morphology: a) Ti atom-centered smallest; b) hollow site-centered small; c) Ti atom-centered middle and d) hollow site-centered large with 9, 16, 25 and 64 formula units per UC, respectively. The distances d_1, d_2, d_3, d_4 between edge oxygen atoms and diameter D_{OO} are shown in b) and c) by twice-terminated arrows. The D_{OO} and D_{TiTi} diameters are shown in c) by twice-terminated arrows. O_1, O_2, O_3, O_4, O_7, O_8, O_9, O_{10} are edge oxygen atoms; O_5 and O_6 are corner oxygen atoms.

Table 1 demonstrates the ability of the M&A force field to reproduce the lattice constants of rutile crystal. The optimization of atomic structure has been done through the minimization of potential energy of the system in the MM calculations with the GULP package[36]. The DFT calculation results are taken from Evarestov and Zhukovskii,[40]. the structure optimization is implemented as the potential energy minimization with the help of

the conjugate gradient algorithm. As one can see, the discrepancy between DFT PBE results and experimental data is 1% and the corresponding discrepancy for the MM simulations with M&A force field is 2%.

Table 1 The lattice constants a and c of optimized TiO_2 rutile bulk.

	Experimental data[52]	Present MM simulations	DFT PBE calculations[40]
a, Å	4.594	4.49	4.65
c, Å	2.959	3.01	2.98

The value of the nanostructure's volume per unit cell is the key parameter for the Young's modulus determination, see Eqs. 4a and 4b. The volume of an unstrained facetted nanowire at a temperature T can be calculated as a product of the period of unit cell, $L_{0,T}$, and the area of the cross-section of NW (Figures 2b and 3), S. The nanowire period is well defined quantity. However, the NW cross-section area cannot be defined unambiguously. The area of the largest FNW cross-section should be a product of the length of NW cross-section (110) facet side and the length of NW cross-section ($1\bar{1}0$) facet side. The length of NW cross-section (110) facet side can be estimated as the distance between nuclei of the two corner oxygen atoms O_1 and O_2, d_{OO}=27.52 Å (Figure 2b). In one's turn the length of the NW cross-section ($1\bar{1}0$) facet side is a distance between two corner oxygen atoms O_2 and O_3, d_{OO}=25.93 Å. On the other hand, the same quantities can also be estimated as the distances between O_4-O_5 atoms and O_6-O_7 ones which are 27.89 Å and 27.88 Å, respectively, Figure 2b. To take into account the size of the oxygen atoms one should also add the quite ambiguous value of the oxygen atom diameter to the obtained values that introduces an extra uncertainty to the cross-section area.

The calculation of volume of other FNWs is else less unequivocal process. The irregularities of the facets surface have noticeable contribution to the nanowire structure. Moreover, the significantly smaller distances between the corner oxygen atoms (for example, in the smallest FNW, Figure 3a) become comparable with the ambiguous atomic diameter.

In the present study we applied the method of nanostructure volume calculation analogous to the one employed in the previous research.[37] At first, the calculation of molar volume V_M of the unstrained largest FNW at T=0 K was performed using the geometrical parameters of the nanowire and the effective anion radius. As in previous study,[37] the effective radius of the three-coordinated oxygen anion R=1.36 Å[53] was chosen for estimating the size of oxygen atom in the nanostructure. The area of the nanowire's cross-section was calculated as a product of ($d_{O_1O_2}$+2R Å) into ($d_{O_2O_3}$+2R Å). Finally, the molar volume was

estimated as a product of the cross-section area and the period of largest FNW $L_{0,T=0}$ divided by the number of TiO_2 formula units per unit cell. The obtained value of V_M is 32.33 $Å^3$. To describe the temperature dependence of the molar volume, the experimentally observed data on the change of the rutile crystal lattice constants with temperature in the interval 15-1280 K were employed.[54-59] A three-degree polynomial was fitted to the 19 points data set as follows:

$$V_M(T)=aT^3+bT^2+cT+d, \tag{11}$$

where a=-3.72·10^{-10} $Å^3K^{-3}$; b=9.13·10^{-7} $Å^3K^{-2}$; c=2.11·10^{-4} $Å^3K^{-1}$; d=31.69 $Å^3$. The volume of any nanostructure under consideration was calculated according to the equation

$$V_M(T)=N_{FU}(aT^3+bT^2+cT+V_M(0)), \tag{12}$$

where N_{FU} is the number of formula units per unit cell of the nanowire or nanotube, and $V_M(0)$=32.33 $Å$ is the molar volume of the largest FNW.
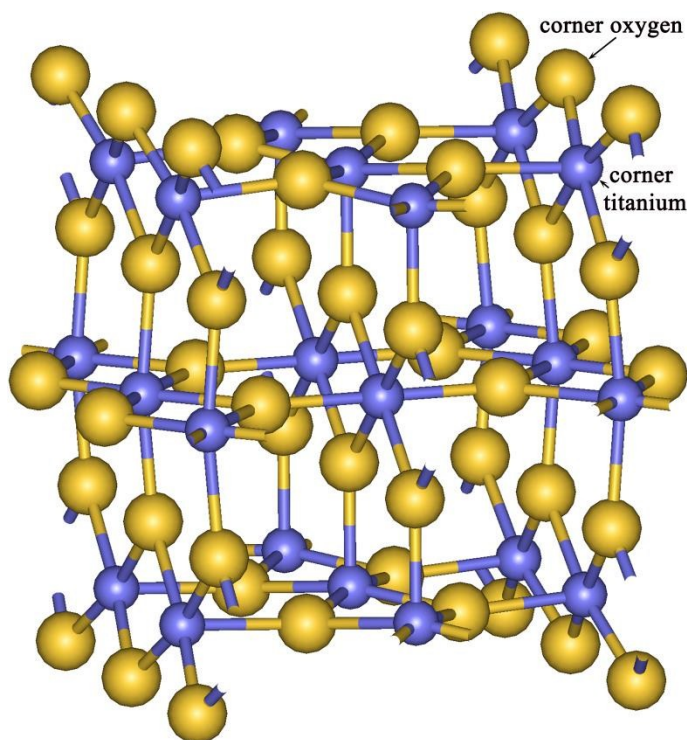

Figure 4. The image of two cells of the smallest nanowire. The two-coordinated surface corner oxygen atom and five-coordinated surface corner titanium atom are marked.

The cylindrical carbon nanotubes have a monoatomic wall and in the case of the Poisson's ratio calculation the only choice of the size D in Eqs. (5) and (6) is the diameter of the nanotube. The facetted nanotubes and nanowires have several structural parameters to be selected as the size D, Figures 1-3.

The aside facets (110) and ($1\bar{1}0$) of the hollow site-centered NWs have similar structures, see Figures 3b and 3d. To measure a distortion perpendicular to the mechanical

load along the NW axis one can choose a distance between two edge oxygen atoms: the distance between O_1 and O_2, d_1, the distance between O3 and O4, d_2, or diagonal (diameter) D_{oo}, see Figure 3b. The aside facets (110) and ($1\bar{1}0$) of the Ti atom-centered NWs have different structures, see Figures 2b, 3a and 3c. Because of this the distance between O_7 and O_8, d_3, and the distance between O_9 and O_{10}, d_4, (see Figure 3c) are different and apparently have different changes under uniaxial stress. The diameter or diagonal D_{oo} may be an integrated parameter relating both facets.

The oxygen atoms of bulk crystal are three coordinated and titanium atoms are six coordinated. The surface corner (bridging) oxygen atoms of NWs are two coordinated while the titanium atoms are five coordinated (Figure 4). It is known[60-62] that the displacements upon the relaxation of the surface bridging oxygen and titanium atoms can differ by as much as 2 times according to the experimental data[60] and 25 times according to the results of ab initio calculations.[61,62]. The similar effect is found here for the displacements of atoms in the ridges of the NW. Consequently, the change of the D_{OO} due to uniaxial stress has a significant contribution of the surface oxygen atom shift besides of the total uniform transverse dilation or compression. To consider the influence of the different surface atoms on the Poisson's ratio we used two diagonals, D_{OO} or D_{TiTi} (see Figures 3b, 3c), as the size D in Eqs. (6), (7) and (10) for the computation of Poisson's ratio (v_{OO} or v_{TiTi}, respectively).

Table 2. The structural properties of optimized CSW NT, four facetted NT, Ti atom-centered and hollow site-centered [001]-oriented NWs.

Nanowire or nanotube size (number of TiO_2 formula units *per* UC)	Present MM simulations			DFT[40]			
	NW or NT period, $L_{0,0}$, Å	Corner Ti-Ti distance D_{TiTi}, Å	Corner O-O distance D_{OO}, Å	NW period, L^*, Å		Corner O-O distance D_{OO}, Å	
				PBE	PBE0	PBE	PBE0
81 (largest)	3.012	35.87	37.81	2.96	2.95	39.27	38.71
64 (large)	3.012	31.39	33.33	2.96	2.95	34.57	34.14
25 (middle)	3.011	17.96	19.97	2.94	2.93	20.71	20.48
16 (small)	3.010	13.50	15.43	2.94	2.92	16.09	15.89
9 (smallest)	3.006	9.03	10.97	2.91	2.88	11.49	11.27
72 (intact)	3.013	34.89	36.59	-	-	-	-
72 (distorted)	3.061	35.84	37.77	-	-	-	-

Table 2 demonstrates the values of the distance between corner titanium atoms and between corner oxygen atoms or diagonal or diameter of the FNWs and FNTs under study (see Figures 2 and 3). As a whole, it follows from Table 2 that the differences between the results of the present simulations and data of DFT large scale study don't exceed 2-3%.

Results and Discussion

The results of our molecular-mechanics simulations demonstrate that CSW NT i. e. distorted four facetted NT has a lower Young's modulus values than that for the four facetted NT. Simultaneously the temperature dependence of the Young's modulus for the distorted four facetted NT displays the more intensive decrease of the stiffness with the temperature increase, see Figure 5. These relations between the elastic characteristics of the two FNTs can easily be attributed to the disturbances which are brought in the structure of the distorted FNT by the fluorite-like elements, Figure 1b, region S. The presence of the fluorite-like elements in rutile structure provides higher coordination numbers for some titanium and oxygen atoms. Also, Figure 6 indicates that the period of the distorted FNT is notably greater than the period of the intact (with regular rutile structure) FNT. This observation, probably, reveals one of the possible stages of the Young's modulus diminishing mechanism: the nanotube with mixed structure has additional number of degrees of freedom to relax under external loading and, consequently, to diminish stiffness.
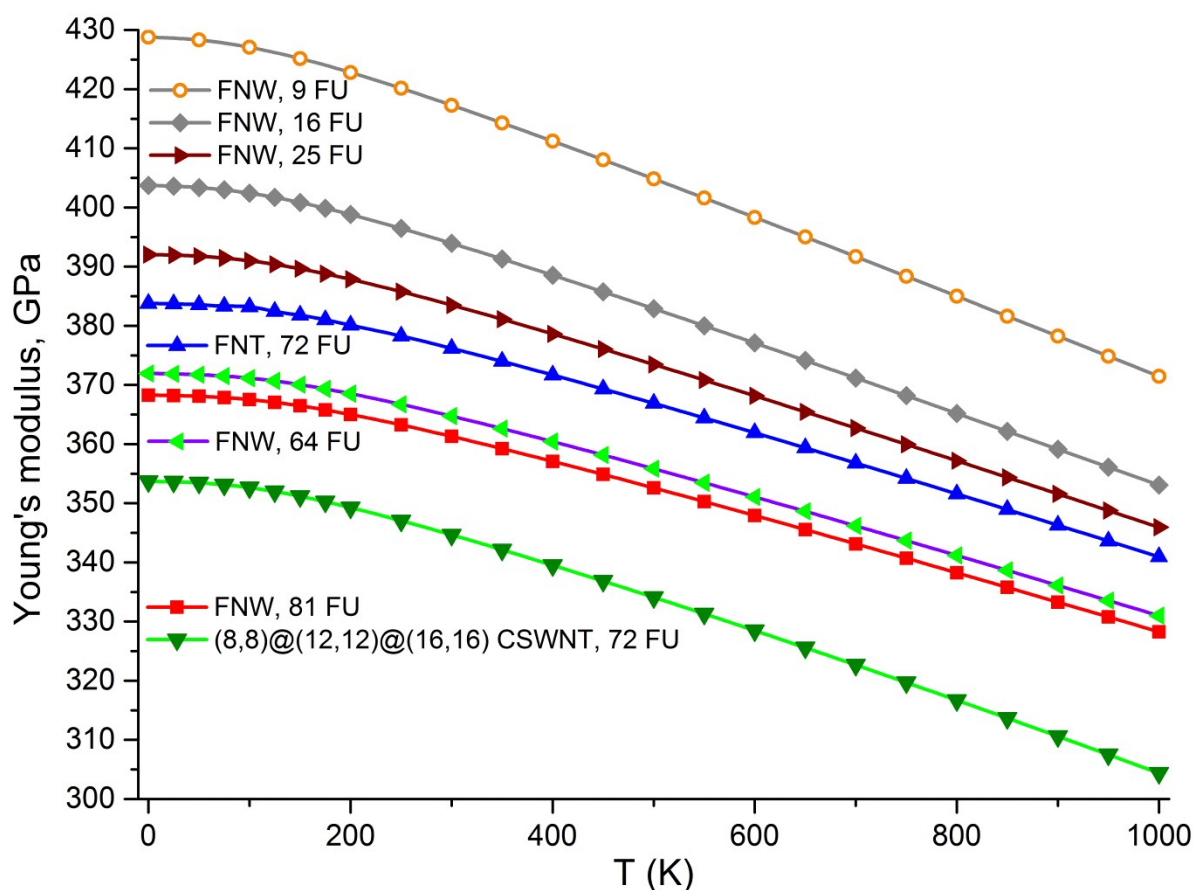

Figure 5. Temperature dependence of the Young's modulus for the CSW NT, four facetted NTs and NWs.

The nanotube pore of the intact facetted nanotube (Figure 2a) can also be treated as a sort of the FNW structure defect which should reduce the stiffness of the FNT relative to the

FNW. As it was aforementioned, the FNT was obtained from largest FNW by cutting a pore. Nevertheless, the Young's modulus for the four facetted NT with 72 formula units per UC exceeds the Young's modulus not only for the largest four facetted NW (81 FU), but also for large NW (64 FU) and is more close to the modulus of the middle FNW with 25 formula units per UC, Figure 5. Also, as it follows from Figure 6, in contrast to the previous case of the relations between two nanotubes, the FNT with greater stiffness has a longer unit cell than the largest FNW (81 FU per UC) and large FNW (64 FU per UC). The temperature dependence of the Young's modulus for the FNT is almost the same as one for the large FNW, see Figure 5 and Table 3. At the same time, the Young's modulus temperature dependence of the distorted FNT is the strongest one from all nanostructures under consideration.

The Young's modulus for the FNWs increases with the decrease of FNW's size. The smaller are the nanowire diameters the greater is the rate of modulus value growth. The difference between the Young's modulus values of nanowires with 81 ($Y(0)$=368 GPa) and 64 ($Y(0)$=371 GPa) FU per UC is small – 1%. The difference is 6% for the small (16 FU) ($Y(0)$=404 GPa) and smallest (9 FU) ($Y(0)$=429 GPa) facetted nanowires. In other words, one needs to heat FNW (64 FU) up to ≈200 K to level the stiffness of this nanowire and the stiffness of the FNW (61 FU) at 0 K. However, in the case of middle FNW the temperature at ≈600 K is necessary.

Table 3 Change, $\Delta=(Y(T=1000 \text{ K})-Y(T=0 \text{ K}))\cdot100/Y(T=0 \text{ K})$, of the Young's modulus values, $Y(T)$, for the FNTs and FNWs and the change, $\Delta=(L_{0,1000}- L_{0,0}))\cdot100/L_{0,0}$, of the FNTs and FNWs period, $L_{0,T}$, in the temperature interval 0-1000 K.

Nanowire or nanotube size (number of TiO$_2$ formula units *per* UC)	distorted FNT	FNT		FNW			
	72	72	81	64	25	16	9
Δ, %, $Y(T)$	13.9	11.2	10.9	11.0	11.8	12.6	13.4
Δ, %, $L_{0,T}$	0.9	0.8	0.8	0.8	0.7	0.7	0.6

The MM simulation with the help of M&A force field gives $Y(0)$=366 GPa in the direction [001] and 154 GPa in the direction [100] for the rutile bulk crystal. The corresponding experimental values of the Young's modulus are 386 and 148 GPa.[63] The differences are -5% and +4% for the Y in the [001] and [100] directions, respectively, which can be treated as the success of M&A parametrization. According to MM simulation result, the minimal Young's modulus value of all [001]-oriented nanowires is $Y(0)$=368 GPa for the largest FNW which is only slightly greater than the corresponding Y for the rutile bulk crystal. Thus, the Young's modulus for the FNWs approaches to the Y for the rutile bulk

14

crystal from above with the increase of nanowire size. At the same time, as it was shown in our study,[33] the Young's modulus values of the cylindrical nanotubes with the armchair chirality grow with the nanotube's diameter and approach to the crystal value from below.
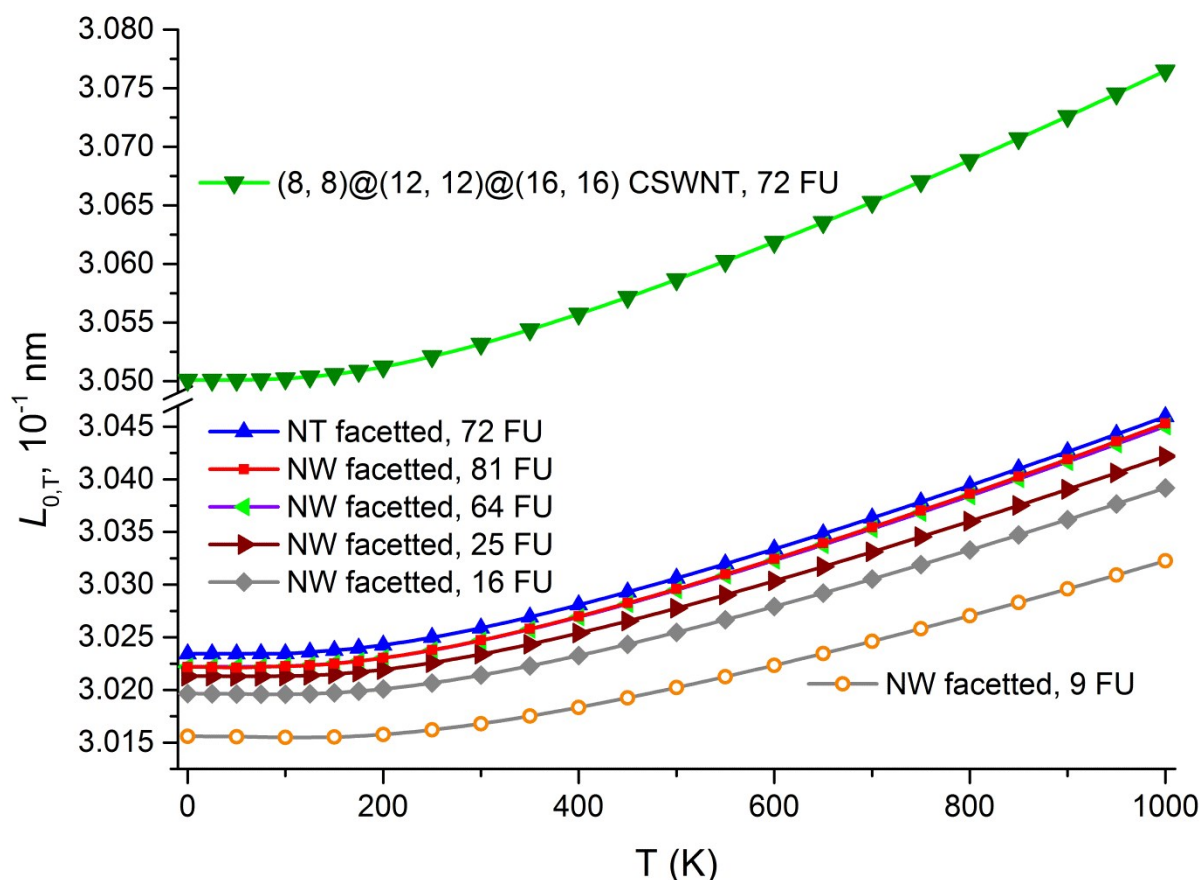

Figure 6. Temperature dependence of the period of the four facetted NTs and NWs.

The Young's moduli for the nanotubes and nanowires decrease with the temperature increase. The temperature dependence of the Young's modulus for the nanowires becomes more steeply with the decrease of nanowire size, Figure 5 and Table 3. All Y versus T curves have a characteristic shape and can be split into two parts. In the temperature interval from 0 to ≈100 K, the Young's modulus decreases rather slowly. The rise of temperature above 150-200 K results in a sensitive increase in the slope of Y versus T.

As in the case of the cylindrical single-walled nanotubes,[33] the behavior of Young's modulus for the FNWs with temperature correlates with the behavior of the period of the nanowires. However, the length of unit cell of the nanowires increases with heating. Nevertheless, the $L_{0,T}$ versus T curves can also be split into two parts. In the temperature range $0 \leq T \leq 150$ K the unit cell length is almost constant, Figure 6. The periods of all the FNWs and FNTs increase as temperature grows in the second range from ≈150 to 1000 K.

15

On the whole, the periods of the FNWs decrease with the size decrease, see Figure 6. However the values of period of the largest FNW (81 formula) and FNW with 64 formula units per UC are close and the corresponding $L_{0,T}$ versus T curves merge in Figure 6.

The average increase of the period for FNTs and large-size FNWs with temperature is about 0.8%, Table 3. The temperature dependence of the FNWs' periods diminishes with the nanowire size decrease. These computational data are close to the experimental values of the rutile lattice vectors temperature dependence. The lattice constant a of the rutile crystal increases by as much as 0.7 % and the lattice constant c increases by as much as 1.1 % with temperature increase from 0 to 1000 K.[48]

The values of the Poisson's ratio for FNTs and FNWs, v_{TiTi} and v_{OO}, calculated using Ti-Ti and O-O diagonals are listed in Table 4. Firstly, from these data one can see that v_{OO} values are greater than v_{TiTi} values. Secondly, the Poisson's ratio v_{OO} is growing with the decrease of the FNW size from largest to smallest. On the contrary, the Poisson's ratio v_{TiTi} demonstrates reverse dependence on NW size. According to v_{TiTi} the compressibility of the FNT is equal to this parameter of the largest FNW (81 FU), but v_{OO} for the FNT is a little lower than this modulus for the largest FNW. Poisson's ratios v_{TiTi} and v_{OO} have a maximal values for the distorted FNT among the considered nanostructures.

Table 4 Poisson's ratio for the TiO_2 based nanotubes and nanowires obtained from OO, v_{OO}, and TiTi, v_{TiTi}, diagonals at T=0 K.

	distorted FNT	FNT		FNW			
Nanowire or nanotube size (number of TiO_2 formula units *per* UC)	72	72	81	64	25	16	9
v_{OO}	0.427	0.282	0.285	0.289	0.302	0.325	0.345
v_{TiTi}	0.351	0.244	0.243	0.240	0.224	0.214	0.200

Both Poisson's ratios decrease in the temperature range 0 to 1000 K for all investigated FNWs and FNT. The decrease is around 1 % for the v_{OO} and a little more for the v_{TiTi} - around 1.5 %. At the same time, the v_{OO} and v_{TiTi} for the distorted FNT demonstrate the 1.2 % growth as the temperature increases from 0 to 1000 K. Interestingly, the temperature behavior of the distorted FNT Poisson's ratios is similar to the one of the bulk crystalline materials and glasses. The v of these structures is known to generally increase with temperature.[35]

Conclusions

The Young's modulus for the [001]-oriented rutile-based four facetted nanowires decreases with the increase of the nanowire size and approaches to the Young's modulus for the rutile bulk crystal from above. The Young's modulus for the four facetted nanotube with

72 formula units per UC obtained from the nanowire with 81 formula units per UC by cutting the rod-like pore, is larger than the modulus for parent nanowire. The Young's modulus for the distorted FNT is less than the modulus for the intact FNT.

The Young's modulus for the FNTs and FNWs decreases with temperature growth. The temperature diminution of the Young's modulus achieves 11-14% and the most significant drop is for the distorted FNT and smallest FNW.

The period of the rutile-based FNWs decreases with the nanowire size decrease. The periods of the similar FNTs are greater than the ones of FNWs and the period of the distorted FNT is significantly longer than others.

The periods of the FNWs and FNTs increase with heating. This increase achieves 0.8% in temperature range 0-1000 K and is in good agreement with the experimental values 0.7-1.1%.

The results of our study indicates that the Poisson's ratio of the TiO_2-based FNTs and FNWs depends on the surface atoms chosen to measure the transverse dimensions of NTs and NWs in the plane normal to the tensile stress axis. This is due to the different degree of relaxation under tensile stress of the chosen surface atoms. In addition, the values of the surface atoms displacements determine the trend of the Poisson's ratio change with the FNW size increase, namely, it may grow or diminish. Apparently, the mentioned effects decrease with the increase of NW size.

The temperature dependence of the v_{OO} and v_{TiTi} for the TiO_2-based FNTs and FNWs is weak. Using the quasi harmonic approximation, the Poisson's ratios for all investigated FNWs and intact FNT tends to decrease by as much as 1-1.5 % with temperature growth from 0 to 1000 K. By contrast, the Poisson's ratios for the distorted FNT increases in the same temperature range.

Acknowledgements

Notes and references

1   S. Kaur, M. Gallei and E. Ionescu, *Adv. Polym. Sci*, 2015, **267**, 143-186.
2   A.W. Tan, B. Pingguan-Murphy, R. Ahmad and S.A. Akbar, *Ceramics International*, 2012, **38**, 4421-4435.
3   L. S. Santos, N. T. C. Oliveira, C. M. Lepienski, C. E. B. Marino and N. K Kuromoto, *revista Matéria,* 2014, **19**, 33-39.
4   A.W. Miles and S. Gheduzzi, *Surgery*, 2012, **30**, 86-91.
5   R. A. Evarestov, D. B. Migas and Yu. F. Zhukovskii, *J. Phys. Chem. C*, 2012, **116**, 13395-13402.
6   Zhenqiang Ye, Huijuan Zhu, Yingying Zheng, Wenjun Dong and Benyong Chen, *Mater. Sci. Eng., A,* 2015, **641**, 281–289.

7   Qingquan Qin, Feng Xu, Yongqing Cao, Paul I. Ro and Yong Zhu, *small* 2012, **8**, 2571-2576.
8   Dayong Jiang, Chunguang Tian, Qingfei Liu, Man Zhao, Jieming Qina, Jianhua Hou, Shang Gao, Qingcheng Liang and Jianxun Zhao, *Mater. Sci. Eng., A*, 2014, **610**,1–4.
9   Syed S. Amin, Shu-you Li, Xiaoxia Wu, Weiqiang Ding and Terry T. Xu, *Nanoscale Res. Lett.*, 2010, **5**, 338–343.
10   L. Borgese, M. Gelfi, E. Bontempi, P. Goudeau, G. Geandier, D. Thiaudière and L.E. Depero, *Surf. Coat. Tech.*, 2012, **206**, 2459–2463.
11   C. Q. Chen, Y. Shi, Y. S. Zhang, J. Zhu and Y. J. Yan, *Phys. Rev. Lett.*, 2006, **96**, 075505.
12   Jin-Yuan Hsieh, Jian-Ming Lu, Min-Yi Huang and Chi-Chuan Hwang, *Nanotechnology*, 2006, **17**, 3920–3924.
13   Chen-Li Zhang and Hui-Shen Shen, *Appl. Phys. Lett.*, 2006, **89**, 081904.
14   Chen-Li Zhang and Hui-Shen Shen, *J. Phys. D: Appl. Phys.*, 2008, **41**, 055404.
15   F. Scarpa, L. Boldrin, H. X. Peng, C. D. L. Remillat and S. Adhikari, *Appl. Phys. Lett.*, 2010, **97**, 151903.
16   N. R. Raravikar, P. Keblinski, A. M. Rao, M. S. Dresselhaus, L. S. Schadler and P. M. Ajayan, *Phys. Rev. B*, 2002, **66**, 235424.
17   G. Dereli and B. Süngü, *Phys. Rev. B*, 2007, **75**, 184104.
18   J.Y. Wu, J.Y. He and Z.L. Zhang, *Comp. Mater. Sci.*, 2013, **80**, 15–26.
19   P. M. Agrawal, B. S. Sudalayandi, L. M. Raff and R. Komanduri, *Comp. Mater. Sci.*, 2006, **38**, 271–281.
20   E. Hernandez, C. Goze, P. Bernier and A. Rubio, *Phys. Rev. Lett.,* 1998, **80**, 4502-4505.
21   H. Jiang Y. Huang and K. C. Hwang, *J. Eng. Mater.-T. ASME,* 2005, **127**, 408-416.
22   R. P. Stoffel, C. Wessel, M.-W. Lumey and R. Dronskowski., *Angew. Chem. Int.Ed. Engl.*, 2010, **49**, 5242-5266.
23   I. Kaplan-Ashiri, S.R. Cohen, K. Gartsman, R. Rosentsveig, G. Seifert and R. Tenne, *J. Mater. Res.*, 2004, **19**, 454-459.
24   I. Kaplan-Ashiri, S. R. Cohen, K. Gartsman, V. Ivanovskaya, T. Heine, G. Seifert, I. Wiesel, H. D. Wagner and R. Tenne, *PNAS,* 2006, **103**, 523-528.
25   M. Griebel, J. Hamaekers and F. Heber, *Comp. Mater. Sci.*, 2009, **45**, 1097-1103.
26   T. Lorenz, D. Teich, J.-O. Joswig and G. Seifert, *J. Phys. Chem. C,* 2012, **116**, 11714-11721.
27   E. W. Bucholz and S. B. Sinnott, *J. Appl. Phys.,* 2012, **112**, 123510.
28   L. Dai, C. H. Sow, C. T. Lim, W. C. D. Cheong and V. B. C. Tan, *Nano Lett.*, 2009, **9**, 576-582.
29   G. Wang and X. Li, *J. Appl. Phys.,* 2008, **104**, 113517.
30   Y.-B. Wang, L.-F. Wang, H. J. Joyce, Q. Gao, X.-Z. Liao, Y.-W. Mai, H. H. Tan, J. Zou, S. P. Ringer, H.-J. Gao and C. Jagadish, *Adv. Mater.*, 2011, **23**, 1356–1360
31   L. Dai, C.H. Sow, C.T. Lim and V.B.C. Tan, in *Nanowires - Fundamental Research*, ed. Abbass Hashim, InTech, University Campus STeP Ri Slavka Krautzeka 83/A 51000 Rijeka, Croatia, 2011, 9, 183-202.
32   A. Gulans and I. Tale, *Phys. Stat. Sol. (c)*, 2007, **4**, 1197-1200.
33   S. I. Lukyanov, A. V. Bandura and R. A. Evarestov, *Phys. Solid State*, 2015, **57**, 2464-2472.
34   L. D. Landau and E. M. Lifshitz, *Course of Theoretical Physics*, **7**: *Theory of Elasticity,* Nauka, Moscow, 1987, Butterworth–Heinemann, Oxford, 1995.
35   G. N. Greaves, A. L. Greer, R. S. Lakes and T. Rouxel, *Nat. Mater.*, 2011, **10**, 823-837
36   J. D. Gale, *Z. Kristallogr.*, 2005, **220**, 552-554.
37   A.V. Bandura, R.A. Evarestov and S.I. Lukyanov, *Phys.Chem.Chem.Phys.*, 2014, **16**, 14781-14791.
38   D.B. Migas, A.B. Filonov, V.E. Borisenko and N.V. Skorodumova, *Phys. Chem. Chem. Phys.*, 2014, **16**, 9490-9498.
39   D.B. Migas, V.L. Shaposhnikov, V.E. Borisenko and F.A. d'Avitaya, *J. Phys. Chem. C,* 2010, **114**, 21013-21019.
40   R.A. Evarestov and Yu.F. Zhukovskii, *Surf. Sci.*, 2013, **608**, 226–240.
41   A. Hallil, R. Tétot, F. Berthier, I. Braems and J. Creuze, *Phys. Rev. B*, 2006, **73**, 165406.
42   C. M. Freeman, J. M. Newsam, S. M. Levinea and C. R. A, Catlow, *J. Mater. Chem.*, 1993, **3**, 531-535.
43   M. O. Zacate, R. W. Grimes and K. Scrivener, *J. Mater. Sci.*, 2000, **35**, 3727-3732.
44   M. Mostoller and J. C. Wang, *Phys. Rev. B*, 1985, **32**, 6773-6785.
45   M. Matsui and M. Akaogi, *Mol. Simul.*, 1991, **6**, 239-244.
46   D.-W. Kim, N. Enomoto, Z. Nakagawa and K. Kawamura, *J. Am. Ceram. Soc.*, 1996, **79**, 1095-1099.
47   V. Swamy and J. D. Gale, *Phys. Rev. B*, 2000, **62**, 5406-5412.
48   X. J. Han, L. Bergqvist, P. H. Dederichs, H. Müller-Krumbhaar, J. K. Christie, S. Scandolo and P. Tangney, *Phys. Rev. B*, 2010, **81**, 134108.
49   S. M. Woodley, P. D. Battle, J. D. Gale and C. R. A. Catlow, *Phys. Chem. Chem. Phys.*, 1999, **1**, 2535-2542.
50   G. Gao, T. Cagın and W. A. Goddard III, *Nanotechnology*, 1998, **9**, 184-191.
51   T. Liang, Y. K. Shin, Y.-T. Cheng, D. E. Yilmaz, K. G. Vishnu, O. Verners, C. Zou, S. R. Phillpot, S. B. Sinnott and A. C. T. van Duin, *Annu. Rev. Mater. Res.*, 2013, **43**, 109-129.
52   F. Labat, Ph. Baranek, Ch. Domain, Ch. Minot and C. Adamo, *J. Chem. Phys.,* 2007, **126**, 154703-154712.
53   R. D. Shannon, *Acta Cryst.,* 1976, **A32**, 751-767.
54   J. K. Burdett, T. Hughbanks, G. J. Miller, J. W. Richardson Jr. and J. V. Smith, *J. Am. Chem. Soc.*, 1987, **109**, 3639-3646.
55   K. Sugiyama and Y. Takeuchi, *Z. Kristallog.*, 1991, **194**, 305-313.
56   R. J. Swope, J. R. Smyth and A. C. Larson, *Am. Mineral.*, 1995, **80**, 448-453.
57   S. C. Abrahams and J. L. Bernstein, *J. Chem. Phys.,* 1971, **55**, 3206-3211.
58   E. P. Meagher and G. A. Lager, *Can. Mineral.,* 1979, **17**, 77-85.
59   H. Seki, N. Ishizawa, N. Mizutani and M. Kato, *Journal of the Ceramic Association, Japan,* 1984, **92**, 219-223.
60   G. Cabailh, X. Torrelles, R. Lindsay, O. Bikondoa, I. Joumard, J. Zegenhagen and G. Thornton, *Phys. Rev. B*, 2007, **75**, 241403.
61   S. J. Thompson and S. P. Lewis, *Phys. Rev. B*, 2006, **73**, 073403.

62   A. V. Bandura, D. G. Sykes, V. Shapovalov, T. N. Troung, J. D. Kubicki and R. A. Evarestov, *J. Phys. Chem. B*, 2004, **108**, 7844-7853.
63   J. B. Wachtman, Jr., W. E. Tefft and D. G. Lam, Jr., *J. Res. NBS. A. Phys. Ch.*, 1962, **66A**, 465-471.

The temperature dependence of the Young's modulus and Poisson's ratio of a number of TiO_2–based four-facetted nanotubes and nanowires are predicted through the calculation of the Helmholtz free energy.